4-2018

Influenza D Virus M2 Protein Exhibits Ion Channel Activity in Xenopus laevis Oocytes

Evan Daniel Kesinger
University of Nebraska-Lincoln, evan.kesinger@huskers.unl.edu

INFLUENZA D VIRUS M2 PROTEIN EXHIBITS ION CHANNEL ACTIVITY IN *Xenopus laevis* OOCYTES

By

Evan Daniel Kesinger

A THESIS

Presented to the Faculty of

The Graduate College at the University of Nebraska

In Partial Fulfillment of Requirements

For the Degree of Master of Science

Major: Biological Sciences

Under the Supervision of Professor Hideaki Moriyama

Lincoln, Nebraska

April, 2018

INFLUENZA D VIRUS M2 PROTEIN EXHIBITS ION CHANNEL ACTIVITY IN *Xenopus laevis* OOCYTES

Evan Daniel Kesinger, M.S.

University of Nebraska, 2018

Advisor: Hideaki Moriyama

The Influenza virus M2 ion channel has good potential as a target for antiviral drugs, as the channel is necessary for viral replication. M2 of Influenza A and B viruses has beenstudied extensively, and is understood to function as a proton channel. Antiviral drugs like amantadine and rimantadine have been used to block the function of Influenza A virus M2. Influenza C virus M2 has also been researched and is understood to act as a chloride ion channel. However, the M2 channel of Influenza D virus (DM2) has been studied very little, and the activity and mechanism of the channel are unknown. To test the function of the channel, the protein was expressed in a *Xenopus laevis* oocyte system, and expression was confirmed with immunofluorescence and mass spectrometry. DM2 expressed in oocytes was analyzed using a two-electrode voltage clamp. The native DM2 protein was tested along with C-terminal altered M2 and M2 altered at an intracellular motif. The native DM2 channel was found to exhibit ion channel activity and chloride specificity comparable to that of Influenza C virus M2, and C-terminal and transmembrane altered M2 was found to exhibit altered ion channel activity from native DM2. These results suggest that DM2 functions as a chloride ion channel.

Table of Contents

Figures and Tables

INTRODUCTION: Literature Review and Aim

1.1 Influenza virus

Influenza virus can infect multiple species of animals, including humans [1, 2], and can cause fever, sneezing, and more serious diseases like pneumonia. While most influenza virus infections have mild symptoms, genetic shift, drift, and reassortment events have resulted in highly pathogenic strains [3]. To date, four influenza virus species have been identified, namely A, B, C, and D [2, 4]. Influenza A infects several different species including humans, as well as porcine, bovine, and canine species [5]. Types B and C infect humans and pigs [6]. Type D is a relatively newly identified type of influenza virus, which has been found to infect cattle and pigs [4]; it was recognized as a new virus type by the International Committee of Taxonomy in 2016 (talk.ictvonline.org).

Influenza D virus infection in cattle is typically asymptomatic [7, 8]. However, its infection in swine can result in clinical disease. Swine can also be infected with all other types of influenza viruses (type A-C). As a result, swine can serve as a “mixing vessel” for highly pathogenic influenza viruses, including those with zoonotic potential into the human population [9] (Figure 1). A recent study has confirmed that people working in close proximity to calves have higher rates of seropositivity to the influenza virus (94%), more so than the general population (1.3%) [10]. Because of the potential for crossover to a human host, it is important to understand the functions of the Influenza D proteome.

1.2 Influenza Virus Life Cycle

Influenza virus begins its life cycle by entering a host cell (Figure 2). The surface of the virus has hemagglutinin (HA), neuramidase (NA), and matrix protein 2 (M2) [13]. HA binds to sialic acid moieties from the receptors on the host cell membrane. Species specificity of Influenza virus infection is determined by the linkages between sialic acids and the carbohydrates shared within their glycoproteins; these linkages are recognized by HA. Human Influenza viruses recognize sialic acids with α(2,6) linkages, avian Influenza virus recognizes sialic acids with α(2,3) linkages, and swine Influenza virus recognizes both types of sialic acids [11]. Binding of HA to the sialic acid receptor triggers receptor-mediated endocytosis, which allows the Influenza virus to enter the cell as an endosome. The acidity of the inside of endosome (pH 5-6) induces fusion between HA and the endosomal membrane; and also then activates the M2 protein. The M2 protein acts as an ion channel to conduct protons and acidify the interior of the viral particle, rupturing it with the endosome and releasing the viral ribonucleoproteins (vRNP) into the cytoplasm [12]. The vRNPs are transported to the host cell nucleus and express their own encoding genes. The produced Influenza proteins are transported to the cell membrane, and bud out of the cell.

1.3 Influenza Virus M2 Protein

M2 is necessary in at least two stages of Influenza virus reproduction (Figure 2). The first stage is the release of vRNPs into the host cell cytoplasm. M2 is responsible for acidifying the virus interior, causing the virus to rupture the endosomal membrane. The second stage is the budding of new viruses from the host cell. It is not yet clear what

mechanism is used by M2, but it has been demonstrated that virus budding is attenuated when the M2 C-terminal domain is mutated [37].

1.4 Molecular Basis of Influenza M2 Ion Channel

The influenza A virus M2 protein (AM2) is involved in the release of viral RNPs from the endosome (uncoating) and the transport of hemagglutinin to the cell surface via the trans-Golgi network [19-21]. In both processes, acidification of the external environment around the virus activates the M2 proton channel capability, thus leading to virus rupture.

The AM2 protein consists of an N-terminal (external) domain, a transmembrane domain, and a C-terminal (internal) domain (Figure 4 and 5). The C-terminal domain is amphipathic, and it has been found to be important for tetramer formation [22,23] and ion conductance [24]. The tandem transmembrane helices of the AM2 monomers turn left at 23° form vertical of the bundle, and there is an inner pore at the center of the tetramer [22]. Methyl groups at Val27 (Figure 5B) keep the opening pore with the diameter of 3.1 Å. The conformation of the channel holds water molecules in the inner pore, which contributes the flow of protons. The pore of the channel is widest at Gly34 with the diameter at 6 Å. The C-terminal region narrows down to 1.7 and 1.4 Å at residues His37 and Trp41, respectively. The Trp41 residues are within van der Waals distance of each other, and are thought to bind in hydrogen bonding to keep the gate closed.

The crystal structure of AM2 has been solved at high-resolution (PDB ID, 4QKL, deposited in the monomer format) [25]. Based on this model, electrophysiological behaviors of the pH-gated M2 proton channel were explained by the simulations [26].

Specifically, Val27 and Ser31 in the amino–terminal and His37 and Trp41 of carboxyl-terminal were shown to act as a hinge and a gate, respectively (HxxxW motif hereafter) [27]. NMR structures of the channel domain of M2 (2L0J; deposited in a tetramer format; Figure 5) [28] were also reported, which were consistent with the structure obtained by the X-ray crystallography.

The Influenza B virus M2 protein (BM2) also contains the HxxxW motif [27], and the protein structure was solved by NMR (2KIX; deposited in a tetramer format) [29].

The Influenza C M2 protein (CM2) was reported by Hongo *et al.* [30] ((C/Yamagata/1/1988); Figure 4), and it was identified as a voltage chloride ion channel [31]. While CM2 does not contain the HxxxW motif, the helical region contains a YxxxK motif found through visual observation (Figure 4). CM2 undergoes a proteolytic intracellular naturalization process that removes the leading 24 amino acids [32]. Mature CM2 consists of an amino-terminal extracellular domain, transmembrane domains, and a carboxyl-terminal internal domain [32, 33]. In a different isolate, (C/Ann Arbor/1/1950) [34], a transmembrane domain, (Tyr27-Val46) was predicted by site-specific infrared dichroism analyses and a global molecular dynamics search [18]. Side chains of Leu31, Leu34, Met41, and Leu44 residues were predicted to point to the center of the tetramer assembly. CM2 undergoes oligomerization by disulfide bonding among Cys1-Cys6-Cys20 [35]. CM2 undergoes glycosylation at Asn11 [32, 33] and palmitoylation at Cys65 [36]. Three amino acid substitutions between Yamagata and Ann Arbor isolates were found to be located outside of the transmembrane domain.

1.5 Biomedical significance

Influenza infection is typically prevented by administering an efficacious vaccine [14, 15]. However, if infection has already occurred, the only treatment option is the use of antivirals. Unfortunately, owing to the inherent instability and high mutation rate of influenza genomes, most current antivirals are no longer effective at inhibiting influenza virus replication. The only currently available anti-viral that targets the Influenza M2 protein ion channel (M2; Figure 4) [16, 17] is called amantadine (PubChem CID, 2130) (Figure 3), and is only partially effective. Thus, there is an urgent need to develop an M2 ion channel blocker capable of suppressing viral infection.

1.6 Aims

The type D proteome (D/Swine/Oklahoma/1334/2011), including the M2 protein, shares more sequence similarity with the type C proteome than with the type A or B proteomes [10]. As such, many of my inferences about the structure and function of the DM2 protein are derived from what we know about CM2. I hypothesized that DM2 has voltage-gated chloride ion channel activity similar to that of CM2, and that this channel might depend on the YxxxK motif present in both channels (Figure 4, 5c). To test the hypothesis, I chose to use the two-electrode voltage-clamp technique (TEVC) technique coupled with a heterologous expression system with *Xenopus* oocytes because this system is well-established.

Chapter II MATERIALS AND METHODS

2.1 Plasmid Construction

A *Xenopus* oocyte expression vector, pNCB1 (GenBank Accession number MF984401), was constructed with pGEMHE used as a base [38], which contains a T7 promoter, *Xenopus laevis* β-globin 5'-UTR, multiple cloning sites, *Xenopus laevis* β-globin 3'-UTR, poly-A sequences. Native CM2 (Locus, YP_089658.1 (C/Ann Arbor/1/50)), and native and modified DM2 (Locus, AFJ19025 ((D/Swine/Oklahoma/1334/2011)) (Figure 4) were synthesized and cloned into pNCB1 (Figure 6). DNA was synthesized and cloned by GenScript (Figure 14; Piscataway, New Jersey, USA).

2.2 cRNA Synthesis

Before cRNA preparation, pNCB1 constructs containing DM2 structural genes were linearized by *Hind*III using a 20 µl reaction volume: 2 µL FastDigest buffer (ThermoFisher, Waltham, Massachusetts), 1 µL HindIII enzyme, 1 µg plasmid DNA, and filled to 20 µL with H_2O. DNA was recovered by ethanol precipitation using 1 µL of 0.5 M EDTA, 2 µL of 4M ammonium acetate, and 46 µL of 100% ethanol, for a total precipitation volume of 69 µL. The mixture was kept at -20˚C for at least 20 minutes. Precipitated DNA was recovered by centrifugation at 21,000 reciprocal centrifugal force (RCF) for 15 minutes at 4℃. After removal of supernatant, the precipitate was dried in air. DNA was dissolved in 10 µL of 10 mM Tris-HCl pH 8.0 1 mM EDTA (TE) buffer. Linearized DNA was stored at -20˚C. Linearized DNA was analyzed using 1% agarose gel electrophoresis (Figure 7). To estimate the concentration of recovered DNA, I used

ImageJ software [39]. The 1 kb GeneRuler DNA ladder (Thermo Fisher) in the same agarose gel was used to obtain the concentration reference.

Invitrogen Ambion mMESSAGE mMACHINE T7 Transcription Kit (Thermo Fisher) was used in the 5'-capped mRNA (cRNA) synthesis: 10 µL 2X NTP/CAP solution, 2 µL 10X reaction buffer, 1 µL T7 RNA polymerase, 0.1-1 µg linearized DNA, and filled to 20 µL with H_2O. mRNA was recovered by precipitation in 30 µL nuclease-free water and 30 µL LiCl kept at -20˚C for 30 min. The cRNA was recovered by centrifugation at 21,000 RCF for 15 min. at 4˚C, rinsing with 70(v/v)% ethanol, and centrifuging again. The recovered cRNA was dissolved in phosphate buffered saline (PBS) consisting of 137 mM NaCl, 2.7 mM KCl, 10 mM Na_2HPO_4, and 1.8 mM KH_2PO_4-HCl pH 7.4. Recovered cRNA was analyzed with agarose gel electrophoresis (Figure 7) and quantified by the Qubit HS RNA Assay system (Thermo Fisher) (Table 1) (Figure 8). cRNA was stored at −20˚C up to 30 days.

2.3 Injection of Xenopus Oocytes with cRNA

Pipettes were pulled with a pipette puller P-97 (Sutter Instrument, Novato, California) to have tips with diameters less than 22.5 µm and lengths of about 2.5 cm. Pipette tips were inspected with the Microforge MF-830 (Narishige International USA, East Meadow, New York) to ensure the tips were smooth at the edges, as to not tear the oocyte membrane, and also to verify that the diameter was acceptable. Defolliculated *Xenopus* oocytes were purchased from *Xenopus* 1 (Dexter, Michigan). Each individual oocyte was placed in ND96 buffer (96 mM NaCl, 2 mM KCl, 1.8 mM $CaCl_2$, 1 mM $MgCl_2$, and 5 mM HEPES-NaOH pH 8.5) [31] and injected with 50.6 nL of cRNA using Auto-

Nanoliter Injector Nanoject II (Drummond Scientific, Broomall, Pennsylvania) (Figure 9). Other oocytes were injected with PBS as a control.

2.4 Immunofluorescent Imaging

I used MYC Mouse Antibody 9E 10 (Developmental Studies Hybridoma Bank, University of Iowa, Iowa City, Iowa) to detect the cMyc-tag at the C-terminus of the construct. Three oocytes injected with cRNA or PBS and left to incubate for five days were fixed in 4% paraformaldehyde and blocked in 5% horse serum in Tris-buffered saline (50 mM Tris; 150 mM NaCl, to pH 7.6 with HCl) (TBS) solution. The oocytes were incubated in 1:500 anti-Myc mouse antibody 9E10 diluted in 1% skim milk in TBS-T solution (TBS containing 0.05% Tween-20), and were then incubated in 1:250 Alexa-Fluor 488 donkey anti-mouse antibody (Thermo Fisher) diluted in 1% skim milk in TBS-T solution. Oocytes were then observed under the Olympus FV500 Confocal Microscope at the Morrison Microscopy Core Research Facility (University of Nebraska-Lincoln).

2.5 Mass Spectrometry of Plasma Membranes

Five *Xenopus* oocytes injected by DM2cMyc cRNA or PBS were incubated for 3 days at 18˚C. Oocytes were then placed in either 20 µL (2 µg) trypsin in 180 µL ND96 buffer or 20 µL trypsin in 180 µL 50 mM ammonium bicarbonate. Each treatment was incubated at 25℃ for 5 h. Aliquots of 5µL were then sampled from each treatment. To remove salts, the sample was subjected to the nanoLC-MS/MS using a 1h gradient on a 0.075mmx250mm C18 Waters CSH column feeding into a Q-Exactive HF mass spectrometer. All MS/MS samples were analyzed using Mascot (Matrix Science, London,

UK; version 2.5.1). Mascot was set up to search the cRAP_20150130 db (113 entries) uniprot-Xenopus_laevis_20170615 db (42878 entries) and a custom database containing our construct sequences. Mascot search was performed with a fragment ion mass tolerance of 0.060 Da, and a parent ion tolerance of 10.0 PPM. Deamidation of asparagine and glutamine, and oxidation of methionine were specified in Mascot as variable modifications. Scaffold (version Scaffold_4.8.1, Proteome Software Inc., Portland, OR) was used to validate MS/MS-based peptide and protein identifications. Peptide identifications were accepted if they could be established at a 1% false discovery rate (FDR) by the Peptide Prophet algorithm [40] with Scaffold deltamass correction. Protein identifications were accepted if they could be established at a 1% FDR and contained at least 1 identified peptide. Protein probabilities were assigned by the Protein Prophet algorithm [41]. This part of work is done with the Proteomics and Metabolomics Core Research Facility (University of Nebraska-Lincoln).

2.6 Two-Electrode Voltage Clamp

Glass electrodes were pulled with the P-97 puller, and broken to about 5 cm. The tips were about 3 mm long and 22.5 µm or less in diameter. Each electrode was filled with filter-sterilized 3 M KCl, and placed on the voltage and current electrode holders for the Oocyte Clamp Amplifier OC-725C (Warner Instruments, Hamden, Connecticut). The OC-725C amplifier was connected to the Digidata 1550A Digitizer (Molecular Devices, Sunnyvale, California) (Table 2). pCLAMP software (Molecular Devices) was configured to perform the voltage clamp experiment (Table 3). Each oocyte was placed in a bath containing ND96 at pH 8.5. The bath electrodes were set and the voltage and

current electrodes were used to puncture the oocyte (Figure 10). pCLAMP software was used to control the holding potential of the oocyte and record the resulting currents. The holding potential was decreased from 60 mV to −200 mV incrementally by −10 mV for two seconds at each step. Measurements of CM2 ended at −130 mV, DM2 at −160 mV, and control at −200 mV, depending on the amplitude of the resulting current. Data analysis was performed using the Boltzmann charge-voltage approximation

$$f(V) = \frac{I_{max}}{\left(1+e^{\frac{V_{mid}-V}{V_C}}\right)} + C$$

where V is membrane potential, I_{max} is maximal current, V_{mid} is potential when current is half-maximal, V_c is voltage required to change current e-fold, and C is constant y-offset. This approximation was done automatically in the pCLAMP program (Molecular Devices) [45, 46], and obtained the membrane potential which gives a half of maximal opening of the ion channel (V_{mid}) as one of the representative values.

CHAPTER III RESULTS AND ANALYSIS

3.1 Detection of DM2 by Mass Spectrometry

Tryptic mass spectrometry [42] was used to confirm the presence of the DM2cMyc protein in *Xenopus* oocytes. Trypsin was added to an aliquot of ND96 medium containing an oocyte injected with cRNA encoding cMyc-tagged DM2. After two hours, a fraction of media was taken, and was passed through a desalting C18 column, and then was subjected to mass spectrometry (Figure 11). The peptide sequence, 35 amino acids, corresponding to the junction area between the amino terminal of the DM2, the spacer, and a portion of cMyc-tag was identified (Figure 4 and 11). In the tryptic mass

spectrometry, the recovery of membrane associated protein is often limited [42]. The identified fragment wasn't protected by the membrane.

3.2 Heterogeneous Gene Expression of Influenza D M2 Protein Using Xenopus Oocyte

A DM2 construct with a carboxyl end cMyc-tag was used to assay the expression of the DM2 protein in *Xenopus laevis* oocytes (Figure 4, S1). DM2 conjugated with the cMyc tag was expressed under the *Xenopus* β-globin 5'-UTR in the pNCB1 vector, which is adapted from pGEMHE [38]. *In vitro* transcribed cRNA was injected into the oocyte, and the oocyte was incubated in ND96 medium at 18˚C for 48 hours. The injected oocytes were subjected to staining to detect the DM2 protein through the cMyc epitope-tag using primary 9E10 antibody and secondary Alexa-Fluor 488 antibody. The stained oocytes were observed through confocal microscopy (Figure 12). A distinct green band was observed in the oocytes injected with cRNA encoding cMyc-tagged DM2, while the control injected with phosphate buffer saline did not show any florescence. This result was consistent with the observation with CM2 by Hongo *et al*. [30], although there were experimental differences, such as that they used the rabbit immune serum against the GST fusion protein containing CM2 protein. Thus, the result indicated that cMyc-tagged DM2 was produced in *Xenopus* oocytes upon injection of the cRNA, and formed a layer near the surface of the oocyte.

3.3 Voltage Gate of DM2 and Mutants

Intact *Xenopus* oocytes (5 total) injected by phosphate buffer saline (PBS) were subjected to the Two Electrode Voltage-Clamp (TEVC) method after 2 days of incubation (Figure 13). The oocyte exhibited an inward current of about -5 μA when the membrane voltage was kept at -200 mV. The behaviors of intact and PBS-injected oocytes were similar, and the injection per se did not seem to change the electrophysiological signature of the oocyte. The inward current was most likely the result of innate voltage-gated chloride channels in the *Xenopus* oocyte [43-46].

Oocytes injected by cRNA encoding DM2cMyc and by PBS were compared by their electrophysiological behaviors using TEVC. The DM2cMyc-expressed oocytes (5 total) showed about -4 μA of inward current at the membrane voltage of -150 mV, while PBS-injected oocytes showed inward current at -0.1 μA (Figure 13). The charge-voltage Boltzmann distribution model was applied to represent the gating voltage as the midpoint of the sigmoid curve, V_{mid} (Table 4). The averaged V_{mid} values, $\langle V_{mid} \rangle$, for DM2 cMyc-injected oocyte and PBS-injected oocyte were -155 ± 11 mV and -200 ± 2mV, respectively. Thus, I interpreted the inward current observed in DM2cMyc RNA-injected oocyte was due to the voltage-gated ion channel activity of the expressed protein. I concluded the same experimental procedure is applicable to other constructs, including DM2 without a tag.

To test if DM2 has ion channel activity, voltage-gated current was observed in five oocytes injected with either RNA encoded by the M2 protein from influenza type C (CM2) or DM2 were subjected to the TEVC (Figure 13). The CM2 construct used in this study provided induced inward current -4.5 μA when the membrane voltage was kept at

-130 mV, which was consistent with previously reported observations by Hongo *et al.* [30, 31]. The DM2 construct gave -3.6 μA of inward induced current at the membrane voltage of -130 mV. The $<V_{mid}>$ for CM2 and DM2 injected oocytes were -141 ± 10 mV and -146 ± 3 mV, respectively.

The ion channel activity of a DM2 variant with an extra 16 amino acids added to the C-terminal tail (DM2a) (Figure 4A) was observed. The channel had an inward current of about -5.5 μA at a holding potential of -170 mV (Figure 13), and had a $<V_{mid}>$ of -168 ± 4 mV (Table 4). DM2 variants were also constructed by GenScript by substituting Y72 and K76 with alanine. Y72A had an inward current of about -7 μA at a holding potential of -110 mV (Figure 13), and had a $<V_{mid}>$ of -103 ± 2 mV (Table 4). K76A had an inward current of about -6 μA at -130 mV (Figure 13), and had a $<V_{mid}>$ of -120 ± 3 mV (Table 4).

A t-test was performed on the $<V_{mid}>$ values to analyze if each construct's gating potential was significantly independent from that of DM2 at $p<0.01$ (Table 4). The t-value of DM2 and PBS-injected was 35.75 and the p-value was < 0.0001, so the DM2 construct was significantly different from the negative control. The t-value of DM2 and CM2 was 0.30 and the p-value was 0.39, so the two constructs were not significantly different. The t-value of DM2 and Y72A was -21.75 and the p-value was < 0.00001, so the two constructs were significantly different. The t-value of DM2 and K76A was -9.32 and the p-value was < 0.00001, so the two constructs were significantly different. The t-value of DM2 and DM2cMyc was 3.19 and the p-value was < 0.01, so the two constructs were significantly different. The t-value of DM2 and DM2a was 12.17 and the p-value was < 0.00001, so the two constructs were significantly different.

3.4 Reversal Potential of DM2 and Mutants

To assess the ionic species penetrating the DM2 ion channel, the reversal potential was measured using two consecutive recordings for each oocyte. The first run was for the monitoring of ion channel activity and activation of the ion channels; and the second run was for the estimation of the reversal potentials. The reversal potential was calculated with the Nernst Equation

$$V_{Eq} = \left(\frac{RT}{zF}\right) \ln\left(\frac{[X]_{out}}{[X]_{in}}\right)$$

where V_{Eq} is the voltage potential, R is the universal gas constant, T is the temperature of the system in Kelvin, z is the valence of the ion, F is the Faraday constant, $[X]_{out}$ is the external concentration of the ion, and $[X]_{in}$ is the internal concentration of the ion. The reversal potentials for CM2 and DM2 were -22 mV and -21 mV, respectively (Table 5). The valence of the ionic species was calculated as -1 in both cases. When the sodium chloride in the ND96 solution (103.6 mM [Cl^-]) was replaced by 96mM sodium methanesulfonic acid (resulted 7.6 mM [Cl^-]), reversal potentials were reduced to be -7 mV and -6 mV for CM2 and DM2 respectively. I concluded that DM2 exhibited the chloride ion channel activity under the same conditions that the CM2 ion channel activity was reproduced, as the reversal potential was lost in the absence of chloride [31].

CHAPTER IV DISCUSSION

4.1 Chloride-Specificity of DM2

The reversal potentials of the ion channels (Table 5) suggest that DM2, Y72A, and K76A conduct chloride ions as CM2 does [31], as their reversal potentials in ND96 solution (103.6 µM Cl-) do not differ significantly. The mutant reversal potentials in chloride-substitute ND96 (7.6 µM Cl-), however, are significantly different from CM2 and DM2. The results suggest the mutations affect the chloride specificity of the ion channel, but the specific mechanism is yet to be determined. Similarly, Influenza A M2 loses proton selectivity when His37 is mutated [50].

4.2 Alteration of C-Terminal domain

The DM2cMyc-injected oocytes showed negatively greater $<V_{mid}>$ than that of native DM2-injected oocytes. The DM2cMyc protein has an extra 13 amino acids at the C-terminal of native DM2, including a space and cMyc tag (Figure 4C). I also hypothesized that the extended C-terminal end of the polypeptide affects the ion channel function. Thus, additional amino acids in the carboxyl end likely contribute to the alteration of the channel function. The contribution of the additional amino acids to the gating voltage seemed negatively correlated to their hydrophobicity (Figure 4C). The C-terminal domain of Influenza A M2 is also necessary for proper ion conductance [24].

4.3 YxxxK motif

The gating activity in M2 proteins involves amino acid side chains, namely the cation-pi interactions [47]. The cation-pi interactions malfunction when one of the components is

missing. In the case of DM2, in the YxxxK motif, Tyr and Lys are potentially charged negatively and positively at pH 8.5, respectively. DM2 is likely to have a different valve mechanism from AM2 because Tyr and Lys are potentially able to form both ionic interactions and cation-pi interactions [48, 49]. With DM2 K76A, the pi provider was removed, so the amino acid remained hydrophobic. In the DM2 Lys76Ala, the cation was removed and a hydrophobic side chain was introduced. Each step requires a certain amount of energy. In both mutated DM2 the gating potential was decreased. The degree of decreased potential was greater in Y72A than K76A (Table 4). This fact may indicate that Tyr72 provides a greater energy barrier than Lys76.

4.4 Future Direction

In this study, I have successfully identified ion channel activity in the Influenza DM2 protein, which is similar to an activity identified in Influenza CM2 (Figure 13) [31]. Altered ion channel activity has been identified in the mutant variants altered at the C-terminal region and the YxxxK motif (Table 4), and the channel has been found to exhibit specificity for chloride ions (Table 5). The YxxxK motif is suspected to have a role in the gating of chloride ions in the channel, but the mechanism has yet to be identified. Specific mechanisms could be determined by solving the 3D structure of the protein, as well as through modeling or molecular dynamics. The protein should also be tested for susceptibility to antiviral drugs like amantadine and rimantadine, which could contribute to the development of drugs to inhibit DM2.

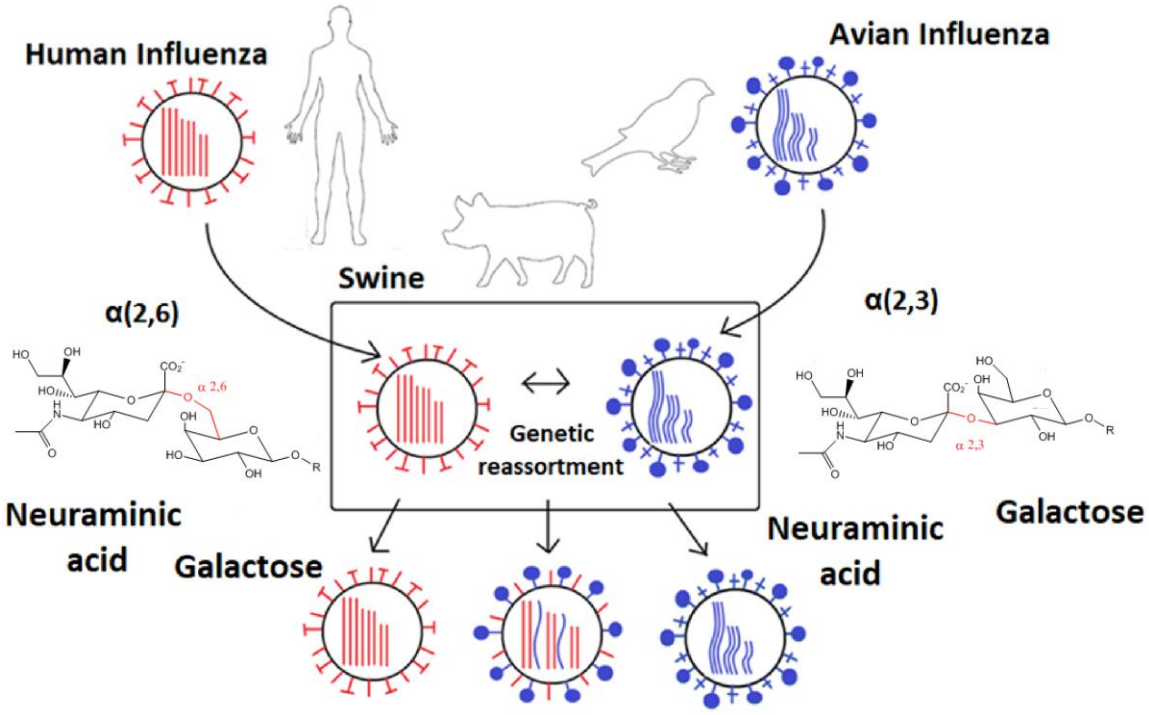

Figure 1: Swine as a mixing vessel for Influenza. Influenza virus has species-specificity based on the linkages of sialic acid moieties on receptors of hosts. Human Influenza virus recognizes the sialic acid with linkage α(2,6), avian Influenza virus recognizes the sialic acids with linkage α(2,3), and swine Influenza virus recognizes both [11]. As swine cells have each sialic acid linkage recognized by avian and human Influenza viruses, human and avian Influenza viruses have the capacity to infect a swine host [9]. This creates an environment in swine where the different Influenza virus species can infect the same cells and potentially engage in genetic reassortment, causing new Influenza types to emerge.

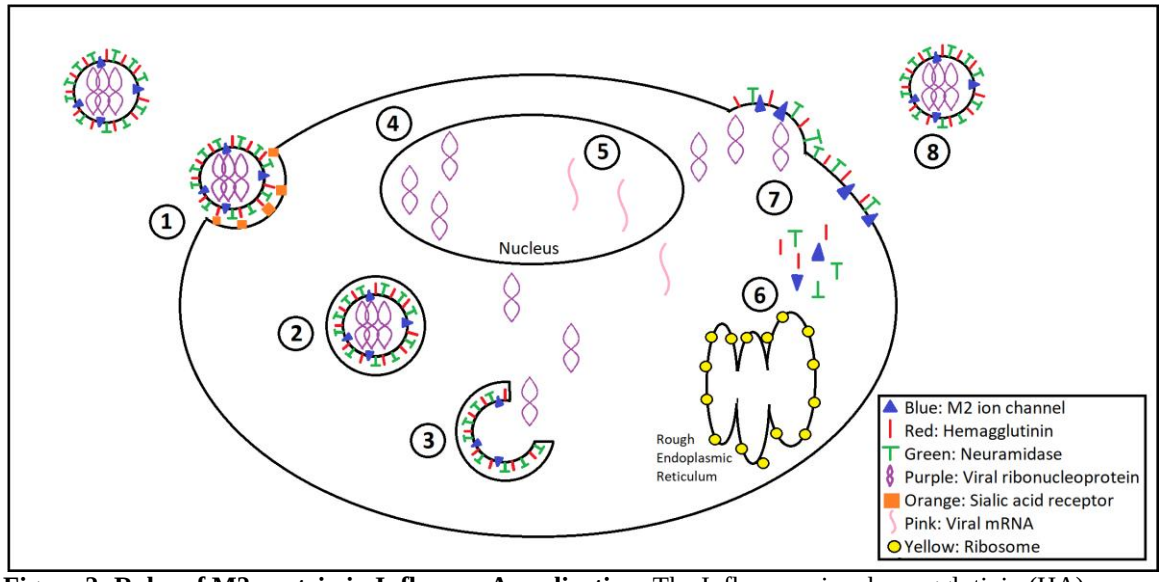

Figure 2: Roles of M2 protein in Influenza A replication. The Influenza virus hemagglutinin (HA) recognizes sialic acid moieties of receptors on the host plasma membrane (1). This triggers receptor-mediated endocytosis of the virus (2). Viral hemagglutinin binds to the endosomal membrane, and the acidic environment of the endosome (pH 5-6) activates the matrix protein 2 (M2) ion channel, leading to rupture of the virus particle and the endosomal membrane (3). The viral ribonucleoproteins are transported to the cell nucleus (4), and viral mRNA is synthesized (5). The viral mRNAs encoded genes are then translated into proteins (6). Viral proteins are transported to the cell membrane with newly synthesized viral ribonucleoproteins (7). New Influenza viruses are budded out of the cell (8). M2 is a critical part of at least two of these stages. The first is the release of vRNPs into the host cell cytoplasm (3). M2 is responsible for channeling ions and acidifying the virus interior, causing the fused endosome to rupture. The second stage is the budding of new viruses from the host cell (7 and 8). M2, along with HA and neuramidase (NA), is required in order for a virus particle to bud properly [13].

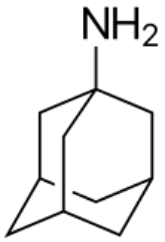

Figure 3: Chemical structure of amantadine. Amantadine (PubChem CID, 2130) is an antiviral drug that inhibits Influenza virus reproduction by blocking the M2 ion channel [16,17]. Amantadine is no longer recommended as an antiviral treatment in the first choice, as the drug is only semi-effective against recent virus types. The drug has been tested against Influenza C, with no evidence for the inhibition of M2 [31].

Figure 4. Amino acid sequences. A. Primary structures of Influenza C virus M2 protein (CM2; Sequence ID, YP_089658.1 (C/Ann Arbor/1/1950)) **and Influenza D virus M2 protein** (DM2; AFJ19025 (D/Swine/Oklahoma/1334/2011)). CM2 contains a 24 amino-acid-signal sequence (−24 to −1). Mature CM2 starts with Cys1, and contains from the amino terminal reported extracellular, transmembrane (underlined), and internal domains. Amino acid substitutions between Yamagata (BAA03793.1 (C/Yamagata/1/1988)) and Ann Arbor isolates were indicated in brackets. CM2 has disulfide-linked oligomerization sites ('*'; Cys1, Cys6, Cys20), a glycosylation site (Asn11, 'g') and a palmitoylation site (Cys65, 'p'). In DM2, the predicted transmembrane domain was indicated by underline. The YxxxK motif, Tyr72 and Lys76 in D, was indicated by the bold face. A C-terminal variant in Dm has a spacer GAG and a cMyc-tag EQKLISEEDL. A C-terminal variant in DM2, DM2a, has an extra peptide from the vector, pNCB1. **B. Structures of M2 proteins.** AM2. M2 protein from Influenza A virus (AAA43303 (A/Udorn/1972(H3N2)) has a NMR structure (residues 22–62; PDB ID, 2L0J) and crystallographic structure (21–46; 4QKL). BM2. M2 protein from Influenza B virus (ACF54325.1 (B/Taiwan/70061/2006)) has a NMR structure (1–33; 2KIX). CM2. M2 protein from Influenza C virus has structures by site-specific infrared dichroism (27–46; [18]). DM2. M2 protein from Influenza D virus is in this study. Solved or predicted structures were underlined. Amino acid residues providing experimental structure information are indicated by underlines. **C. Predicted secondary structure and the hydrophobicity value, GRAVY, of carboxyl ends in DM2 constructs**. Predicted secondary structures E and H correspond to β-strand and α-helix, respectively. In GRAVY, greater positive values indicate higher hydrophobicity.

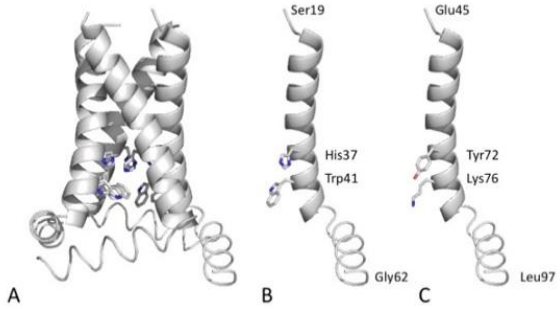

Figure 5. 3D-structure of M2 protein. A. The structure of AM2 was solved experimentally by nuclear magnetic resonance spectroscopy (NMR; structures were deposited in Protein Data Bank with the ID cede 2L0J; the NMR structure contains multiple structures and shown is model 1 out of 8 is shown). The AM2 adopts a homo-tetramer configuration, and the middle of the assembly contains a pre. The valve residues, His37 and Trp41, face inward within the pore on each monomer. B. The monomer structure of AM2 with valve resides, which control ion flow by pseudo-cation-pi interaction. C. A theoretical model of DM2 in monomer format.

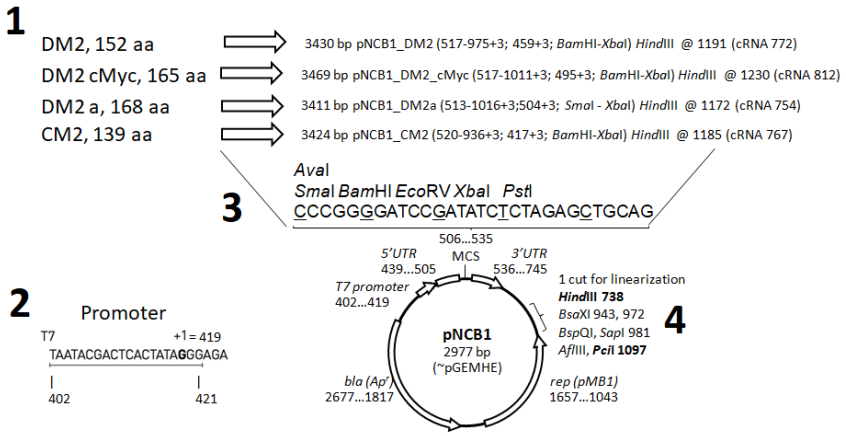

Figure 6: pNCB1 plasmid vector. 1. Plasmid construction. DM2, DM2cMyc, and CM2 were each cloned into the pNCB1 vector with the *Bam*HI and *Xba*I sites. DM2a was cloned into pNCB1 using *Sma*I and *Xba*I. The DM2, DM2cMyc, DM2a, and CM2 genes encode 152, 165, 168, and 139 amino acids, respectively, and their structural genes are 459, 495, 504, and 417 bp, respectively. The *Hind*III linearization locations and lengths for synthesized cRNA for each respective plasmid construct are also shown. 2. The sequence of the T7 promoter. The +1 of cRNA synthesis was shown. 3. Restriction sites. The multiple cloning sites locates between the 5'UTR and 3'UTR regions. The cut sites are noted by the underline. 4. The physical map of the pNCB1. The vector had several cut sites available for linearization. *Hind*III 738 and *Pci*1 1097 were utilized in this research.

Table 1: The amount of synthesized cRNA.

Synthesized cRNA	Quantification	Volume	Total amount
CM2	140 ng/µL	10 µL	1400 ng
DM2	292 ng/µL	10 µL	2920 ng
DM2a	128 ng/µL	10 µL	1280 ng
DM2cMyc	232 ng/µL	10 µL	2320 ng

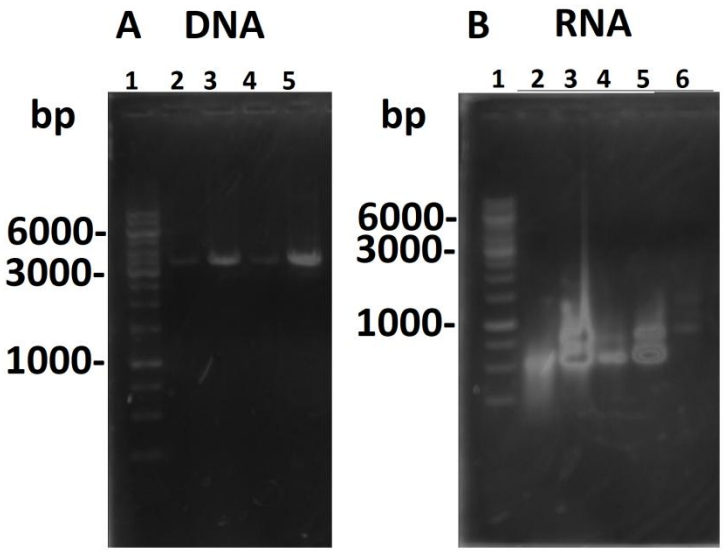

Figure 7: Agarose gel electrophoresis of linearized DNA and cRNA. A. Linearized plasmid vectors by *Hind*III. Recovered DNAs were analyzed by 1% agarose gel electrophoresis. For each lane, 3 µL sample was loaded. Lanes were: 1, the 1 kb GeneRuler ladder; 2, CM2; 3, DM2; 4, DM2a; and 5, DM2cMyc. The length of plasmid vectors were ranged between 3411 bp and 3469 bp. B. Synthesized cRNA. cRNA was analyzed by the same electrophoresis conditions. Lanes were: 1, 1 kb GeneRuler ladder; 2, CM2; 3, DM2; 4, DM2a; 5, DM2cMyc.

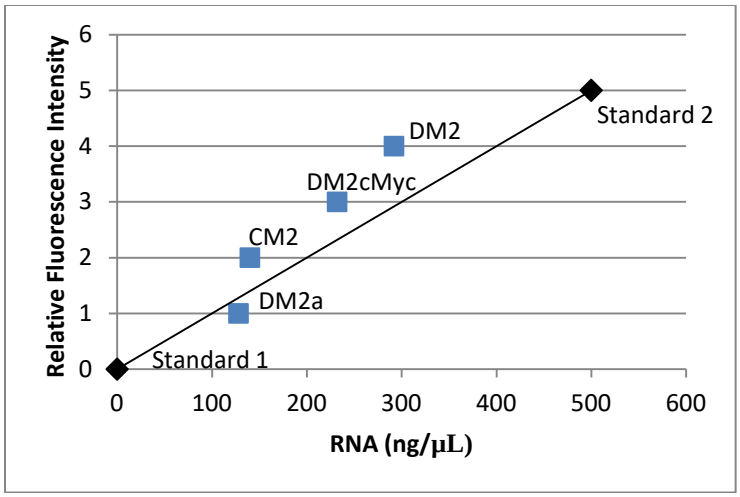

Figure 8: Fluorometer sample quantification. The intensity of fluorescence was calibrated using vendor provided a 0 ng/µL standard and a 500 ng/µL standard (indicated by diamonds). The intensity of fluorescence for each sample was measured (solid squares).

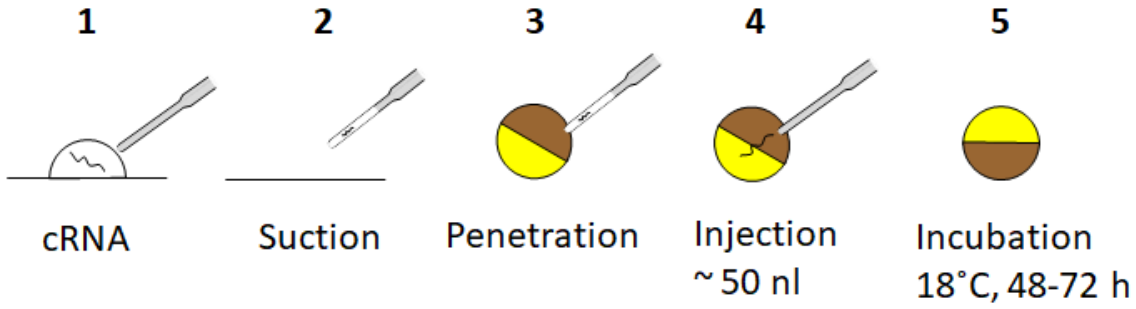

Figure 9: Nanoinjection of *Xenopus* oocyte. cRNA suspended in 1 M PBS solution (1) was brought into a glass pipette (2) secured on the nanoinjector. The nanoinjector was used to penetrate the glass pipette into healthy *Xenopus* oocytes resting in ND96 pH 8.5 solution kept at about 4℃ (3), and then used to inject the cRNA (50.6 nL) into the oocyte (4). The injected oocyte was then incubated at 18℃ for 48-72 hours (5) to allow the injected cRNA to be translated and expressed in the oocyte.

Table 2: Connections for OC-725C and Digidata devices.

OC-725C	Digidata
GAIN TELEGRAPH OUTPUT	GAIN TELEGRAPH INPUT #3
I MONITOR	ANALOG IN #0
V_M x 10	ANALOG IN #1
COMMAND IN ÷10	ANALOG OUT #0

Table 3: pCLAMP configurations.

Navigation	Configuration/Selection
1. Configure/Telegraphed Instrument	
1a. INPUT CHANNELS	Analog input #0
1b. TELEGRAPH INSTRUMENT	OC-725C
1c. TELEGRAPH CONNECTIONS	Telegraph input 3
2. Configure/Lab Bench	
2a. Input Signals	
2a.i. DIGITIZER CHANNELS/Analog IN #0	
2a.i.1. SIGNALS	Add 'Current'
2a.i.2. SCALING	Signal units µA
	Scale factor 1 V/µA
2a.ii. DIGITIZER CHANNELS/Analog IN #1	
2a.ii.1. SIGNALS	Add 'Voltage'
2a.ii.2. SCALING	Signal units mV
	Scale factor 0.01 V/mV
2b. Output Signals	
2b.i. DIGITIZER CHANNELS/Analog IN #0	
2b.i.1. SIGNALS	Add 'Holding'
2b.i.2. SCALING	Signal units mV
	Scale factor 100 mV/V
3. Acquire/Edit Protocol	
3a. Mode/Rate	Acquisition Mode set to 'Episodic'
3b. Inputs	Channel #0, select 'Current'
	Channel #1, select 'Voltage'
3c. Outputs	Channel #0, select 'Holding'

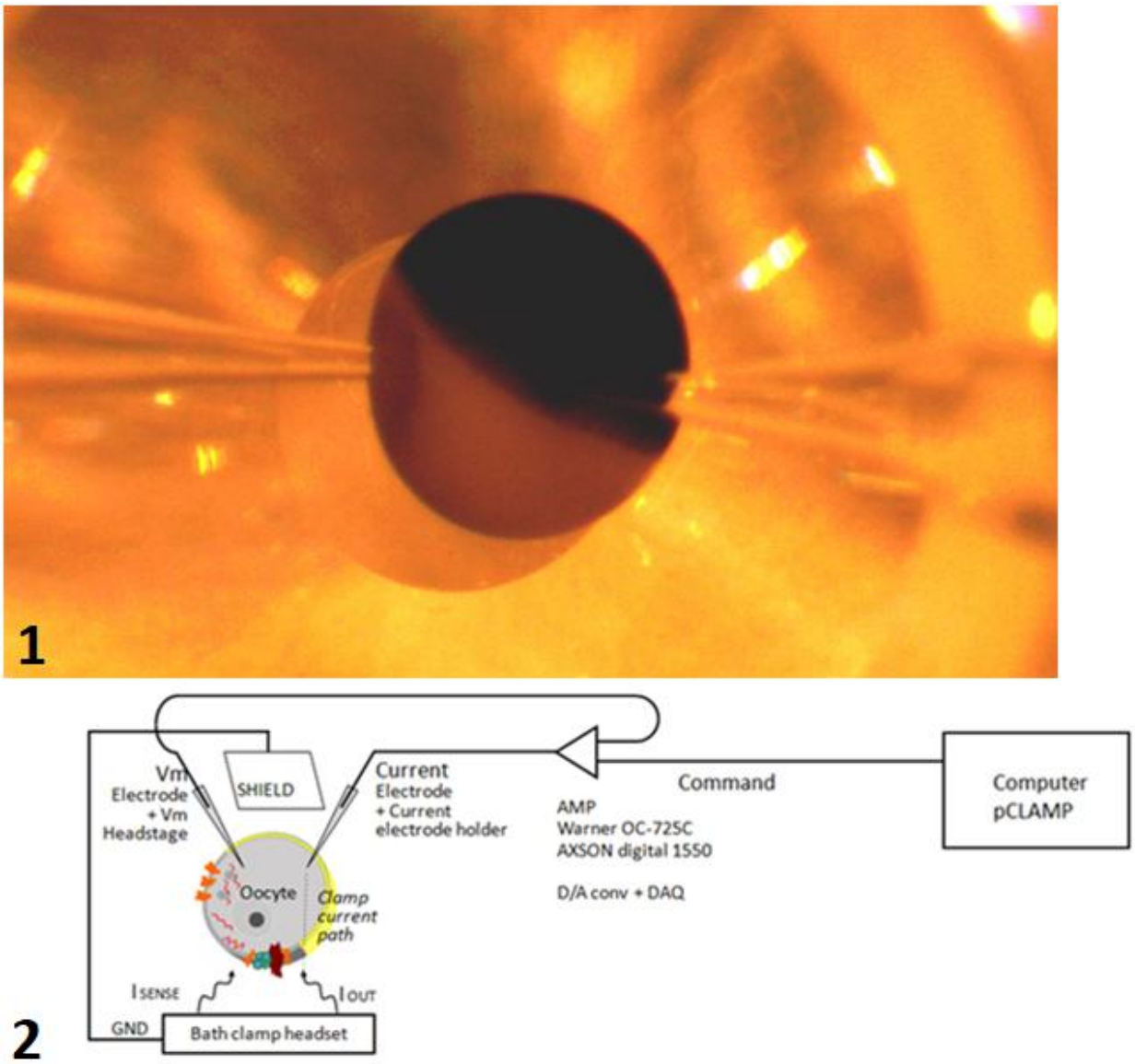

Figure 10: Two-electrode voltage clamp setup. 1. An oocyte in ND96 solution with its membrane impaled by the voltage and current electrodes of the voltage clamp. Only slight dimpling should occur in the oocyte membrane after impalement. 2. Each component of the voltage clamp is listed in the figure. The voltage clamp was connected to the computer with pCLAMP installed via an amplifier, and the pCLAMP software was used to automatically command the holding potential of the oocyte and record the changes in current. The Vm (voltage of the membrane) electrode was secured by the Vm headstage, and held the oocyte's membrane at a constant (holding) voltage. The current electrode was secured by the current electrode holder, and was responsible for compensating for the current generated by the oocyte to maintain the holding potential and to deliver data to pCLAMP. The bath clamp headset maintained a virtual ground with Isense and Iout electrodes placed in the oocyte bath. The aluminum shield acted as a Faraday cage to block external electrostatic noise (if necessary) and was connected to the bath clamp.

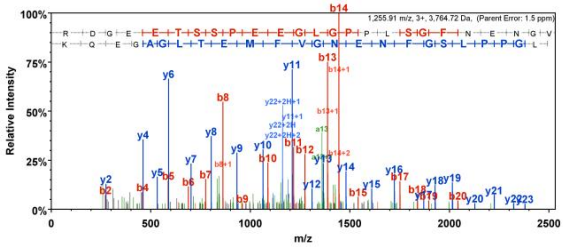

Figure 11. Mass spectrometry and the peptide identification. Trypsin was added to a ND96 medium containing an oocyte injected by RNA encoding c-Myc tagged DM2. Mass spectrometry identified the C-terminal region, RDGEETSSPEEGLGPPLSGFNENGVFMETLGAGEQK, which contains a partial cMyc sequence (Figure 1).

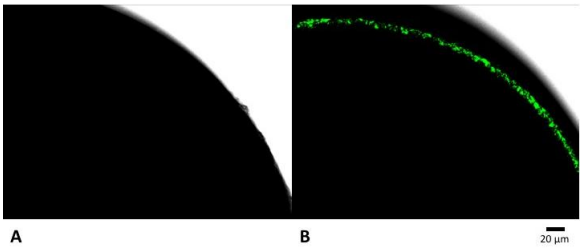

Figure 12. Confocal microscopic photography of oocytes. A. An oocyte injected by phosphate buffer saline. B. An oocyte injected by RNA encoding c-Myc tagged DM2. Oocyte were treated by anti-cMyc antibody (mouse 9E10) and then by donkey anti-mouse Alexa-Fluor 488 antibodies.

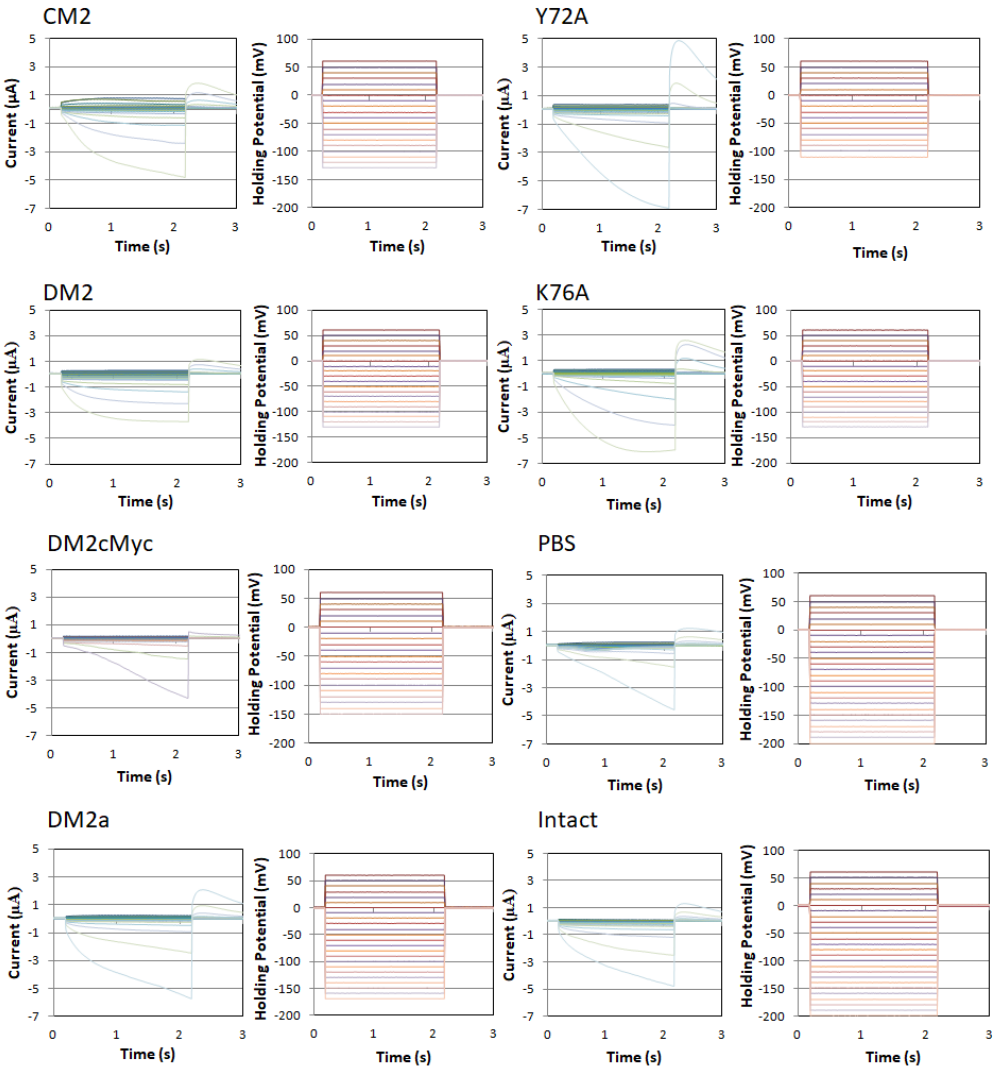
CM2
Y72A
DM2
K76A
DM2cMyc
PBS
DM2a
Intact
Current (µA)
Holding Potential (mV)
Time (s)

A

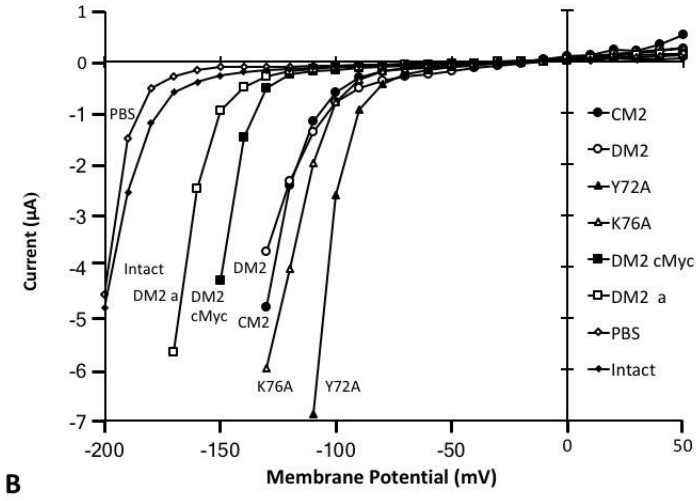

Figure 13. Induced current recorded by Two-electrode voltage-clamp at pH 8.5. A. Induced current (I) and given membrane potential (Vm) over time. An oocyte injected by either RNA or phosphate buffer saline was subjected to the TEVC recording, and the current measurement during the holding potential was given for 2 s. A relax time, 5 s, was given before the next measurement. **B. Plots for induced current and the membrane potential; typical single measurements**.
$<V_{mid}>$: Mean simulated membrane potential which gives a half of ion channel opens (V_{mid}) by the charge-voltage Boltzmann distribution model. Correlation Coefficients in the Boltzmann curve fit was at least 0.85.

Table 4. The charge-voltage Boltzmann distribution model in Two-electrode voltage clamp (N=5). A t-test was performed on each <V_{mid}> to test if it was significantly different from the <V_{mid}> of DM2 at *$p < 0.01$.

Sample	<Vmid> / mV	N.
CM2	-141 ± 10	5
DM2	-139 ± 3	5
DM2 Y72A	-103 ± 2*	5
DM2 K76A	-120 ± 3*	5
DM2cMyc	-155 ± 11*	5
DM2a	-168 ± 4*	5
PBS	-203 ± 2*	5

Table 5. Reversal potential (RP; N=5).

M2	RP in ND96 (mV)	RP in ND96 replaced Cl (mV)
DM2	-20.95 ± 1.05	-5.84 ± 0.40
DM2 Y72A	-21.77 ± 0.77	-9.75 ± 1.97
DM2 K76A	-21.19 ± 1.34	-14.03 ± 2.34
CM2	-22.05 ± 1.19	-6.52 ± 2.06

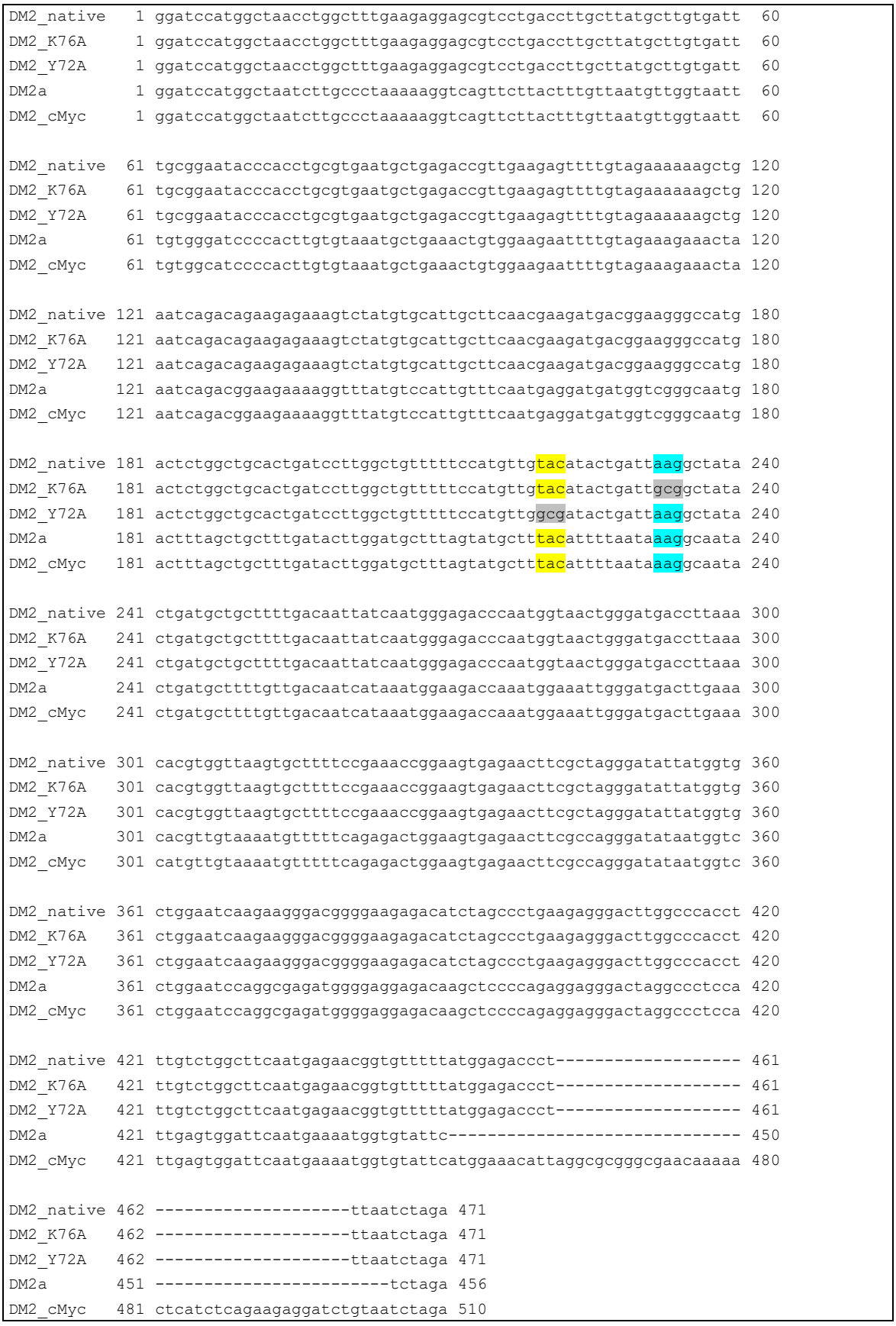
DM2_native 1 ggatccatggctaacctggctttgaagaggagcgtcctgaccttgcttatgcttgtgatt 60
DM2_K76A 1 ggatccatggctaacctggctttgaagaggagcgtcctgaccttgcttatgcttgtgatt 60
DM2_Y72A 1 ggatccatggctaacctggctttgaagaggagcgtcctgaccttgcttatgcttgtgatt 60
DM2a 1 ggatccatggctaatcttgccctaaaaaggtcagttcttactttgttaatgttggtaatt 60
DM2_cMyc 1 ggatccatggctaatcttgccctaaaaaggtcagttcttactttgttaatgttggtaatt 60
DM2_native 61 tgcggaatacccacctgcgtgaatgctgagaccgttgaagagttttgtagaaaaaagctg 120
DM2_K76A 61 tgcggaatacccacctgcgtgaatgctgagaccgttgaagagttttgtagaaaaaagctg 120
DM2_Y72A 61 tgcggaatacccacctgcgtgaatgctgagaccgttgaagagttttgtagaaaaaagctg 120
DM2a 61 tgtgggatccccacttgtgtaaatgctgaaactgtggaagaattttgtagaaagaaacta 120
DM2_cMyc 61 tgtggcatccccacttgtgtaaatgctgaaactgtggaagaattttgtagaaagaaacta 120
DM2_native 121 aatcagacagaagagaaagtctatgtgcattgcttcaacgaagatgacggaagggccatg 180
DM2_K76A 121 aatcagacagaagagaaagtctatgtgcattgcttcaacgaagatgacggaagggccatg 180
DM2_Y72A 121 aatcagacagaagagaaagtctatgtgcattgcttcaacgaagatgacggaagggccatg 180
DM2a 121 aatcagacggaagaaaaggtttatgtccattgtttcaatgaggatgatggtcgggcaatg 180
DM2_cMyc 121 aatcagacggaagaaaaggtttatgtccattgtttcaatgaggatgatggtcgggcaatg 180
DM2_native 181 actctggctgcactgatccttggctgtttttccatgttgtacatactgattaaggctata 240
DM2_K76A 181 actctggctgcactgatccttggctgtttttccatgttgtacatactgattgcggctata 240
DM2_Y72A 181 actctggctgcactgatccttggctgtttttccatgttggcgatactgattaaggctata 240
DM2a 181 actttagctgctttgatacttggatgctttagtatgcttacattttaataaaggcaata 240
DM2_cMyc 181 actttagctgctttgatacttggatgctttagtatgcttacattttaataaaggcaata 240
DM2_native 241 ctgatgctgcttttgacaattatcaatgggagacccaatggtaactgggatgaccttaaa 300
DM2_K76A 241 ctgatgctgcttttgacaattatcaatgggagacccaatggtaactgggatgaccttaaa 300
DM2_Y72A 241 ctgatgctgcttttgacaattatcaatgggagacccaatggtaactgggatgaccttaaa 300
DM2a 241 ctgatgcttttgttgacaatcataaatggaagaccaaatggaaattgggatgacttgaaa 300
DM2_cMyc 241 ctgatgcttttgttgacaatcataaatggaagaccaaatggaaattgggatgacttgaaa 300
DM2_native 301 cacgtggttaagtgcttttccgaaaccggaagtgagaacttcgctagggatattatggtg 360
DM2_K76A 301 cacgtggttaagtgcttttccgaaaccggaagtgagaacttcgctagggatattatggtg 360
DM2_Y72A 301 cacgtggttaagtgcttttccgaaaccggaagtgagaacttcgctagggatattatggtg 360
DM2a 301 cacgttgtaaaatgtttttcagagactggaagtgagaacttcgccagggatataatggtc 360
DM2_cMyc 301 catgttgtaaaatgtttttcagagactggaagtgagaacttcgccagggatataatggtc 360
DM2_native 361 ctggaatcaagaagggacggggaagagacatctagccctgaagagggacttggcccacct 420
DM2_K76A 361 ctggaatcaagaagggacggggaagagacatctagccctgaagagggacttggcccacct 420
DM2_Y72A 361 ctggaatcaagaagggacggggaagagacatctagccctgaagagggacttggcccacct 420
DM2a 361 ctggaatccaggcgagatggggaggagacaagctccccagaggagggactaggccctcca 420
DM2_cMyc 361 ctggaatccaggcgagatggggaggagacaagctccccagaggagggactaggccctcca 420
DM2_native 421 ttgtctggcttcaatgagaacggtgtttttatggagaccct---------- 461
DM2_K76A 421 ttgtctggcttcaatgagaacggtgtttttatggagaccct---------- 461
DM2_Y72A 421 ttgtctggcttcaatgagaacggtgtttttatggagaccct---------- 461
DM2a 421 ttgagtggattcaatgaaaatggtgtattc---------- 450
DM2_cMyc 421 ttgagtggattcaatgaaaatggtgtattcatggaaacattaggcgcgggcgaacaaaaa 480
DM2_native 462 ----------ttaatctaga 471
DM2_K76A 462 ----------ttaatctaga 471
DM2_Y72A 462 ----------ttaatctaga 471
DM2a 451 ----------tctaga 456
DM2_cMyc 481 ctcatctcagaagaggatctgtaatctaga 510

```
DM2_native   1 MANLALKRSVLTLLMLVICGIPTCVNAETVEEFCRKKLNQTEEKVYVHCFNEDDGRAMTL  60
DM2_Y72A     1 MANLALKRSVLTLLMLVICGIPTCVNAETVEEFCRKKLNQTEEKVYVHCFNEDDGRAMTL  60
DM2_K76A     1 MANLALKRSVLTLLMLVICGIPTCVNAETVEEFCRKKLNQTEEKVYVHCFNEDDGRAMTL  60
DM2a         1 MANLALKRSVLTLLMLVICGIPTCVNAETVEEFCRKKLNQTEEKVYVHCFNEDDGRAMTL  60
DM2_cMyc     1 MANLALKRSVLTLLMLVICGIPTCVNAETVEEFCRKKLNQTEEKVYVHCFNEDDGRAMTL  60

DM2_native  61 AALILGCFSMLYILIKAILMLLLTIINGRPNGNWDDLKHVVKCFSETGSENFARDIMVLE 120
DM2_Y72A    61 AALILGCFSMLAILIKAILMLLLTIINGRPNGNWDDLKHVVKCFSETGSENFARDIMVLE 120
DM2_K76A    61 AALILGCFSMLYILIAAILMLLLTIINGRPNGNWDDLKHVVKCFSETGSENFARDIMVLE 120
DM2a        61 AALILGCFSMLYILIKAILMLLLTIINGRPNGNWDDLKHVVKCFSETGSENFARDIMVLE 120
DM2_cMyc    61 AALILGCFSMLYILIKAILMLLLTIINGRPNGNWDDLKHVVKCFSETGSENFARDIMVLE 120

DM2_native 121 SRRDGEETSSPEEGLGPPLSGFNENGVFMETL---------------- 152
DM2_Y72A   121 SRRDGEETSSPEEGLGPPLSGFNENGVFMETL---------------- 152
DM2_K76A   121 SRRDGEETSSPEEGLGPPLSGFNENGVFMETL---------------- 152
DM2a       121 SRRDGEETSSPEEGLGPPLSGFNENGVFSRAADLVTTKPASRTPEWSL 168
DM2_cMyc   121 SRRDGEETSSPEEGLGPPLSGFNENGVFMETLGAGEQKLIS---EEDL 165
```

Figure 14. MAFFT alignment of DM2 native, DM2 Y72A, DM2 K76A, DM2a, and DM2cMyc DNA and amino acid sequences. The yellow highlighted codons correspond to Tyr72 of DM2. The blue highlighted codons correspond to Lys76 of DM2. The gray highlighted codons correspond to the Ala substitutions in Tyr72Ala and Lys76Ala. Each nucleotide sequence begins with its *Bam*HI cloning site (GGATCC) and ends with its *Xba*I cloning site (TCTAGA).

Literature Cited

1. Taubenberger JK, Morens DM. Influenza viruses: breaking all the rules. MBio. 2013;4(4). doi: 10.1128/mBio.00365-13. PubMed PMID: 23860766; PubMed Central PMCID: PMCPMC3735197.

2. Ritchey MB, Palese P, Kilbourne ED. RNAs of influenza A, B, and C viruses. J Virol. 1976;18(2):738-44. PubMed PMID: 944790; PubMed Central PMCID: PMCPMC515602.

3. Taubenberger JK, Morens DM. The pathology of influenza virus infections. Annu Rev Pathol. 2008;3:499-522. doi: 10.1146/annurev.pathmechdis.3.121806.154316. PubMed PMID: 18039138; PubMed Central PMCID: PMCPMC2504709.

4. Hause BM, Ducatez M, Collin EA, Ran Z, Liu R, Sheng Z, et al. Isolation of a novel swine influenza virus from Oklahoma in 2011 which is distantly related to human influenza C viruses. PLoS Pathog. 2013;9(2):e1003176. doi: 10.1371/journal.ppat.1003176. PubMed PMID: 23408893; PubMed Central PMCID: PMCPMC3567177.

5. Parrish CR, Murcia PR, Holmes EC. Influenza virus reservoirs and intermediate hosts: dogs, horses, and new possibilities for influenza virus exposure of humans. J Virol. 2015;89(6):2990-4. doi: 10.1128/JVI.03146-14. PubMed PMID: 25540375; PubMed Central PMCID: PMCPMC4337525.

6. Ran Z, Shen H, Lang Y, Kolb EA, Turan N, Zhu L, et al. Domestic pigs are susceptible to infection with influenza B viruses. J Virol. 2015;89(9):4818-26. doi: 10.1128/JVI.00059-15. PubMed PMID: 25673727; PubMed Central PMCID: PMCPMC4403465.

7. Hause BM, Collin EA, Liu R, Huang B, Sheng Z, Lu W, et al. Characterization of a novel influenza virus in cattle and Swine: proposal for a new genus in the Orthomyxoviridae family. MBio. 2014;5(2):e00031-14. doi: 10.1128/mBio.00031-14. PubMed PMID: 24595369; PubMed Central PMCID: PMC3958797.

8. Ferguson L, Olivier AK, Genova S, Epperson WB, Smith DR, Schneider L, et al. Pathogenesis of Influenza D Virus in Cattle. J Virol. 2016;90(12):5636-42. doi: 10.1128/JVI.03122-15. PubMed PMID: 27030270; PubMed Central PMCID: PMCPMC4886773.

9. Hass J, Matuszewski S, Cieslik D, Haase M. The role of swine as "mixing vessel" for interspecies transmission of the influenza A subtype H1N1: a simultaneous Bayesian inference of phylogeny and ancestral hosts. Infect Genet Evol. 2011;11(2):437-41. doi: 10.1016/j.meegid.2010.12.001. PubMed PMID: 21163369.

10. White SK, Ma W, McDaniel CJ, Gray GC, Lednicky JA. Serologic evidence of exposure to influenza D virus among persons with occupational contact with cattle. J Clin Virol. 2016;81:31-3. doi: 10.1016/j.jcv.2016.05.017. PubMed PMID: 27294672.

11. Skehel JJ, Wiley DC. 2000. Receptor binding and membrane fusion in virus entry: the influenza hemagglutinin. *Annu Rev Biochem*. 69:531–569.

12. Pinto LH, Lamb RA. 2006. The M2 proton channels of influenza A and B viruses. *J Biol Chem*. 281(14):8997–9000.

13. Nayak DP, Balogun RA, Yamada H, Zhou ZH, Barman S. Influenza virus morphogenesis and budding. Virus Res. 2009;143(2):147–161.

14. Rewar S, Mirdha D, Rewar P. Treatment and Prevention of Pandemic H1N1 Influenza. Ann Glob Health. 2015;81(5):645-53. doi: 10.1016/j.aogh.2015.08.014. PubMed PMID: 27036721.

15. Committee On Infectious D. Recommendations for Prevention and Control of Influenza in Children, 2017 - 2018. Pediatrics. 2017. doi: 10.1542/peds.2017-2550. PubMed PMID: 28870977.

16. Samji T. Influenza A: understanding the viral life cycle. Yale J Biol Med. 2009;82(4):153-9. PubMed PMID: 20027280; PubMed Central PMCID: PMCPMC2794490.

17. Wang J, Wu Y, Ma C, Fiorin G, Wang J, Pinto LH, et al. Structure and inhibition of the drug-resistant S31N mutant of the M2 ion channel of influenza A virus. Proceedings of the National Academy of Sciences of the United States of America. 2013;110(4):1315-20. doi: 10.1073/pnas.1216526110. PubMed PMID: 23302696; PubMed Central PMCID: PMCPMC3557100.

18. Kukol A, Arkin IT. Structure of the influenza C virus CM2 protein transmembrane domain obtained by site-specific infrared dichroism and global molecular dynamics searching. J Biol Chem. 2000;275(6):4225-9. PubMed PMID: 10660588.

19. Bron R, Kendal AP, Klenk HD, Wilschut J. Role of the M2 protein in influenza virus membrane fusion: effects of amantadine and monensin on fusion kinetics. Virology. 1993;195(2):808-11. doi: 10.1006/viro.1993.1435. PubMed PMID: 8337846.

20. Ciampor F, Thompson CA, Grambas S, Hay AJ. Regulation of pH by the M2 protein of influenza A viruses. Virus Res. 1992;22(3):247-58. PubMed PMID: 1626420.

21. Ciampor F, Bayley PM, Nermut MV, Hirst EM, Sugrue RJ, Hay AJ. Evidence that the amantadine-induced, M2-mediated conversion of influenza A virus hemagglutinin to the low pH conformation occurs in an acidic trans Golgi compartment. Virology. 1992;188(1):14-24. PubMed PMID: 1566569.

22. Schnell JR, Chou JJ. Structure and mechanism of the M2 proton channel of influenza A virus. Nature. 2008;451:591–595.

23. Salom D, Hill BR, Lear JD, DeGrado WF. pH-dependent tetramerization and amantadine binding of the transmembrane helix of M2 from the influenza A virus. Biochemistry. 2000;39:14160–14170.

24. Tobler K, Kelly ML, Pinto LH, Lamb RA. Effect of cytoplasmic tail truncations on the activity of the M(2) ion channel of influenza A virus. J Virol. 1999;73:9695–9701.

25. Thomaston JL, Alfonso-Prieto M, Woldeyes RA, Fraser JS, Klein ML, Fiorin G, et al. High-resolution structures of the M2 channel from influenza A virus reveal dynamic pathways for proton stabilization and transduction. Proceedings of the National Academy of Sciences of the United States of America. 2015;112(46):14260-5. doi: 10.1073/pnas.1518493112. PubMed PMID: 26578770; PubMed Central PMCID: PMCPMC4655559.

26. Liang R, Swanson JM, Madsen JJ, Hong M, DeGrado WF, Voth GA. Acid activation mechanism of the influenza A M2 proton channel. Proceedings of the National Academy of Sciences of the United States of America. 2016. doi: 10.1073/pnas.1615471113. PubMed PMID: 27791184; PubMed Central PMCID: PMCPMC5111692.

27. Pielak RM, Chou JJ. Influenza M2 proton channels. Biochim Biophys Acta. 2011;1808(2):522-9. doi: 10.1016/j.bbamem.2010.04.015. PubMed PMID: 20451491; PubMed Central PMCID: PMCPMC3108042.

28. Sharma M, Yi M, Dong H, Qin H, Peterson E, Busath DD, et al. Insight into the mechanism of the influenza A proton channel from a structure in a lipid bilayer. Science. 2010;330(6003):509-12. doi: 10.1126/science.1191750. PubMed PMID: 20966252; PubMed Central PMCID: PMCPMC3384994.

29. Wang J, Pielak RM, McClintock MA, Chou JJ. Solution structure and functional analysis of the influenza B proton channel. Nat Struct Mol Biol. 2009;16(12):1267-71. doi: 10.1038/nsmb.1707. PubMed PMID: 19898475; PubMed Central PMCID: PMCPMC3148584.

30. Hongo S, Sugawara K, Nishimura H, Muraki Y, Kitame F, Nakamura K. Identification of a second protein encoded by influenza C virus RNA segment 6. J Gen Virol. 1994;75 (Pt 12):3503-10. doi: 10.1099/0022-1317-75-12-3503. PubMed PMID: 7996141.

31. Hongo S, Ishii K, Mori K, Takashita E, Muraki Y, Matsuzaki Y, et al. Detection of ion channel activity in Xenopus laevis oocytes expressing Influenza C virus CM2 protein. Arch Virol. 2004;149(1):35-50. doi: 10.1007/s00705-003-0209-3. PubMed PMID: 14689274.

32. Pekosz A, Lamb RA. The CM2 protein of influenza C virus is an oligomeric integral membrane glycoprotein structurally analogous to influenza A virus M2 and influenza B virus NB proteins. Virology. 1997;237(2):439-51. doi: 10.1006/viro.1997.8788. PubMed PMID: 9356355.

33. Hongo S, Sugawara K, Muraki Y, Kitame F, Nakamura K. Characterization of a second protein (CM2) encoded by RNA segment 6 of influenza C virus. J Virol. 1997;71(4):2786-92. PubMed PMID: 9060633; PubMed Central PMCID: PMCPMC191402.

34. Muraki Y, Washioka H, Sugawara K, Matsuzaki Y, Takashita E, Hongo S. Identification of an amino acid residue on influenza C virus M1 protein responsible for formation of the cord-like structures of the virus. J Gen Virol. 2004;85(Pt 7):1885-93. doi: 10.1099/vir.0.79937-0. PubMed PMID: 15218173.

35. Muraki Y, Okuwa T, Himeda T, Hongo S, Ohara Y. Effect of cysteine mutations in the extracellular domain of CM2 on the influenza C virus replication. PLoS One. 2013;8(4):e60510. doi: 10.1371/journal.pone.0060510. PubMed PMID: 23593230; PubMed Central PMCID: PMC3617168.

36. Muraki Y, Okuwa T, Furukawa T, Matsuzaki Y, Sugawara K, Himeda T, et al. Palmitoylation of CM2 is dispensable to influenza C virus replication. Virus Res. 2011;157(1):99-105. doi: 10.1016/j.virusres.2011.02.013. PubMed PMID: 21352864.

37. Chen BJ, Leser GP, Jackson D, Lamb RA. The influenza virus M2 protein cytoplasmic tail interacts with the M1 protein and influences virus assembly at the site of virus budding. J Virol. 2008;82(20):10059–10070.

38. Liman ER, Tytgat J, Hess P. Subunit stoichiometry of a mammalian K+ channel determined by construction of multimeric cDNAs. Neuron. 1992;9(5):861-71. PubMed PMID: 1419000.

39. Schneider CA, Rasband WS, Eliceiri KW. NIH Image to ImageJ: 25 years of image analysis. Nature Methods. 2012. 9:671-675.

40. Keller, A et al Anal. Chem. 2002;74(20):5383-92

41. Nesvizhskii, Al et al Anal. Chem. 2003;75(17):4646-58

42. Nakachi M, Moriyama H, Hoshi M, Matsumoto M. Acrosome reaction is subfamily specific in sea star fertilization. Dev Biol. 2006;298:597-604. PubMed PMID: 16934796.

43. Parker I, Miledi R. A calcium-independent chloride current activated by hyperpolarization in Xenopus oocytes. Proc R Soc Lond B Biol Sci. 1988;233(1271):191-9. PubMed PMID: 2454476.

44. Kowdley GC, Ackerman SJ, John JE, 3rd, Jones LR, Moorman JR. Hyperpolarization-activated chloride currents in Xenopus oocytes. J Gen Physiol. 1994;103(2):217-30. PubMed PMID: 7514644; PubMed Central PMCID: PMCPMC2216841.

45. Schroeder JI. Heterologous expression of higher plant transport proteins and repression of endogenous ion currents in Xenopus oocytes. Methods Cell Biol. 1995;50:519-33. PubMed PMID: 8531821.

46. Miller AJ, Zhou JJ. Xenopus oocytes as an expression system for plant transporters. Biochim Biophys Acta. 2000;1465(1-2):343-58. PubMed PMID: 10748264.

47. Gallivan JP, Dougherty DA. Cation-pi interactions in structural biology. Proceedings of the National Academy of Sciences of the United States of America. 1999;96(17):9459-64. PubMed PMID: 10449714; PubMed Central PMCID: PMCPMC22230.

48. Prajapati RS, Sirajuddin M, Durani V, Sreeramulu S, Varadarajan R. Contribution of cation-pi interactions to protein stability. Biochemistry. 2006;45(50):15000-10. doi: 10.1021/bi061275f. PubMed PMID: 17154537.

49. Wintjens R, Lievin J, Rooman M, Buisine E. Contribution of cation-pi interactions to the stability of protein-DNA complexes. Journal of molecular biology. 2000;302(2):395-410. doi: 10.1006/jmbi.2000.4040. PubMed PMID: 10970741.

50. Wang C, Lamb RA, Pinto LH. Activation of the M2 ion channel of influenza virus: a role for the transmembrane domain histidine residue. Biophys J. 1995;69:1363–1371.